Fabrication and Characterization of Thermocouple Probe for Use in Intracellular Thermometry

Manjunath C. Rajagopal[1], Krishna V. Valavala, Dhruv Gelda, Jun Ma, Sanjiv Sinha

Department of Mechanical Science and Engineering, University of Illinois at Urbana-Champaign, USA

Abstract

Measuring temperatures within a biological cell requires a sensor with small thermal mass and microscale or smaller size that is electrically and chemically inert to the cell's environment, and is thermally isolated from the surroundings. We investigate how such requirements can be satisfied in a microscale thermocouple probe that is fabricated using the techniques of silicon-based microelectromechanical systems. Previous reports of invasive probes lacked either the required spatial resolution ($< 5\ \mu$m) or response time (< 4 ms). Here, we report 1 μm thick silicon nitride supported probes with a 5 μm tip that has a response time of 32 μs. These figures enable future transient thermometry of cell organelles. To reduce calibration errors, we devise an on-chip calibration in a vacuum cryostat. We find that the accuracy of our measurements is ± 54 mK for 300 ± 10 K. This work paves the way toward future thermometry at a subcellular level.

Keywords: Microelectromechanical systems, sensors, thermocouple, intracellular measurements.

Email address: `chinnap2@illinois.edu` (Manjunath C. Rajagopal)

[1]Corresponding author

https://doi.org/10.1016/j.sna.2018.02.004

1. Introduction

Temperature is a fundamental thermodynamic property affecting every biochemical reaction in cellular environments. Living cells undergo temperature mediated activities such as cell division [1], gene expression [2], protein stabilization [3], and metabolism [4, 5]. Extracellular thermometry has been shown to be important in detecting cancer [6] and thyroid related diseases [7], and for understanding multiple metabolic pathways [8]. In comparison, thermometry at the subcellular level is relatively less explored. The dominant heat generation reactions inside a cell include the mitochondrial respiratory chain (non-shivering), and the reactions that consume ATP (shivering), both of which are the primary modes of thermal regulations in warm-blooded animals [9]. Temperature gradients can be established within a cell by the reactions associated with multiple organelles in a cell. The nucleus, mitochondria, and centrosomes have been found to be at a temperature of 0.5-1 °C higher than cytoplasm [10]. In addition to gradients, temperature transients also arise, for example, when a cell is subjected to external stimuli such as light [11], drugs [12], or during sudden neurophysiological activities in neuron cells [13]. To understand the physiology of such reactions, there is a growing interest in the measurements of intracellular temperatures, especially in adipose tissues, muscles, and neurons. Since the cell wall and cytoplasm smoothen out the temperature fluctuations arising within the cell, an intracellular probe is necessary for such measurements.

Intracellular thermometry can be invasive or non-invasive. Typically, non-invasive techniques rely on fluorescence lifetimes or intensities that are temperature dependent. Okabe et al [10] used the fluorescence lifetime of a polymer to map temperatures in a cell with an estimated calibration resolution of 0.18-0.58 K. However, the accuracy of measurement was greatly reduced by the presence of a significant temperature gap between the optical setup in the microscope and the sample. The resulting errors were estimated to be as high as 0.35-1.3 K [10]. In a different study, a bio-compatible Green Fluorescent Protein (GFP) has been used as an intracellular temperature probe by using its Fluorescence Polarization Anisotropy (FPA) [14]. The FPA of GFP was calibrated for thermometry using a temperature controlled bath with an accuracy of 0.4 K. However, the readings within a cell show an error of 1.2 K over few seconds of laser heating [14]. Recently, fluorescence intensity of quantum dots has been used to measure intracellular temperature variations in a neuron [15]. It was observed that each quantum dot particle of the same type exhibited different sensitivities of the fluorescence intensity to temperature. Since it was not possible to follow a single quantum dot for both calibration and measurements, a mean sensitivity obtained from calibration of multiple quantum dots was used in the measurements. This serves to reduce the accuracy of the measurements. The reported measurement uncertainty is around 1 K. Non-invasive thermometry techniques typically have accuracies $\gtrsim 1$ K. They also suffer from non-specific signals recorded as temperature. Such signals arise from photobleaching [15], variations in ion concentrations, pH, and microscale viscosity changes within the cell milieu [16].

Invasive thermometry utilizes a chemically inert sensor that is typically formed using a micropipette. One of the earliest attempts involved platinum wires inside micropipettes that were coated on the outside with gold to form a thermocouple junction at the tip [17]. Watanabe et al [18] made a similar attempt but with both metals coating the outside of a micropipette. These earlier studies did not report any sensible measurements in biological cells. Recent attempts involved thermocouple junctions in microcapillaries [19] or tungsten-based thermocouple probes [20, 21]. However, both approaches suffer from critical deficiencies. Metal-filled microcapillaries have been reported to have a thermal time constant around 600 ms [19], which is two orders of magnitude larger than the typical time constants of action potentials in neuron cells [22]. Tungsten-based probes have a junction that is 7-10 μm [20] in length at the tip. This is problematic for cells with typical size 10 μm. Another issue is that past work utilized a water bath for calibration [19, 23, 21] where local convection effects, temperature differences between the reference sensor and the probe, as well as errors from the reference sensor introduce calibration errors. While these error are insignificant in typical applications, they gain significance when measuring small ($\lesssim$ 500 mK) temperature changes in intracellular thermometry. In summary, current sensing techniques measure temperature changes in excess of $\sim$ 1 K with no emphasis on smaller gradients or transient responses.

An invasive intracellular thermometer should be smaller than $\sim$ 5 μm to avoid fatal cell damage [24]. A further restriction on size arises from the fact that transient responses of interest occur on time scales $\lesssim$4 ms [22]. The latter places a constraint on the thermal mass of the sensor. In this paper, we design and fabricate a thermocouple junction, 1 μm in diameter, on a suspended silicon nitride cantilever of 5 μm tip diameter for measuring intracellular temperature changes *in vitro*. The design yields thermal time constant as small as 32 μs. The junction diameter of 1 μm offers spatial resolution sufficient for intracellular measurements. We avoid using a water bath for calibration, and instead devise an on-chip calibration using a gold resistor on the chip. We show that the calibration error can be reduced to be comparable to the noise floor. The fabrication process allows for batch fabrication, making it possible to produce multiple (16 in this work) probes from a 4-inch silicon wafer. The paper is organized as follows. Section 2 presents the fabrication steps. Section 3 discusses the technique used for on-chip calibration. Section 4 discusses testing of the probe and provides estimates of the time constant of the probe.

2. Fabrication

Starting from a double-side polished (100) wafer that is p-doped to a resistivity of 10-20 Ω.cm, we deposited a stress-free, 1 μm thick silicon nitride using Plasma Enhanced Chemical Vapor Deposition (PECVD) on STS Mesc Multiplex PECVD operated at a mix of 13.56 MHz and 380 kHz. The silicon nitride layer, as shown in Fig. 1a, forms the material for the cantilever that eventually supports the metal lines forming a thermocouple. Among common cantilever materials such as silicon carbide, doped silicon, and flexible polymers [25], we chose silicon nitride for this work since it provides excellent thermal isolation

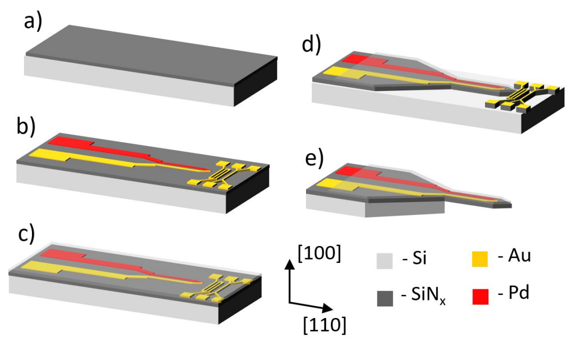

Figure 1: Fabrication of the probe starts with a) deposition of SiN_x using PECVD, followed by b) deposition of thermocouple metal lines, and resistors for calibration. The thermocouple is calibrated as discussed in section 3. This is followed by c) deposition of a thin SiN_x layer to protect the thermocouple, d) reactive ion etching of SiN_x to get the required profile using a patterned photoresist mask, and finally, e) aq. KOH etching of silicon to suspend the probe.

of the thermocouple junction from the base of the cantilever, and is also an electrical insulator. Its compression strength of ∼600 MPa [26] with an Young's modulus of ∼152 GPa [27] enable the cantilever to easily overcome a cell wall's puncture stress of ∼1 MPa [28].

Electron beam metal evaporation (Temescal FC-2000 deposition system) was used to deposit 70 nm thick, 400 nm wide gold and palladium films on top of the 1 μm thick silicon nitride layer. The films were defined using a combination of UV photolithography (Karl Suss MJB3) and electron beam lithography (Raith eLine) to the dimensions of the thermocouple. We chose gold and palladium for the thermocouple since they are resistant to KOH etching that is subsequently used to release the cantilever.

Following the deposition of the metal films for the thermocouple, 300 nm thick metal films were deposited to form heaters and thermometers for calibrating the thermocouple junction, as shown in Fig. 1b. The reference thermometer and thermocouple junction were both 6 μm away from heater. We calibrated the thermocouple prior to releasing the probe from the wafer. After calibration, we deposited a 200 nm thick PECVD silicon nitride layer on top of Si/SiN_x/metal-junction to protect the calibrated thermocouple junction. The second nitride layer, shown as a translucent layer in Fig. 1c, protects the chrome adhesion layer used for metal lines from aqueous KOH etching. A photoresist was patterned to the desired shape of the probe. Using the photoresist as a mask, the nitride was etched using Reactive Ion Etching (PlasmaLab systems Freon RIE) until silicon was exposed. Multiple RIE steps were performed until a profile such as the one shown in Fig. 1d was obtained. The protective nitride layer only at the contact pads was etched away carefully to expose contact pads for electrical connections. The metal electrodes that were used for calibration were unaffected by RIE. However, they were removed in the subsequent step.

The design of the metal electrodes, and the pattern of the probe profile ensure that the tip is oriented along [110]. The nitride tip that extends along [110] has a convex edge, and is on top of the silicon substrate. These features collectively enhance the etch rate of silicon under the tip when aq. KOH is used. Bulk silicon etching was performed using 45% aq. KOH at 80 °C bath temperature. The samples were held by clamps for about 40-50 minutes while etching. By the end of the etch process, a tip of length ∼451 μm was suspended, as shown in Fig. 1e. Figure 2 shows an SEM image of the fabricated probe. Silicon nitride being a poor thermal conductor, isolates the tip from temperature fluctuations in the silicon substrate, and therefore from the external surroundings. During intracellular thermometry, we expect only the suspended part to enter the cell, which enhances thermal isolation. Electrical continuity of the probe after suspension was verified by measuring the thermocouple's resistance before and after etching. Further tests to verify the probe's measurements are discussed in Section 4.

3. Calibration

In previous work, thermocouples for cellular thermometry were calibrated in a water bath. However, as discussed in Section 1, this can lead to significant error due to convection effects in calibration for a probe meant to measure $\lesssim$ 500 mK changes. Here, we avoid this issue through an *in situ* calibration

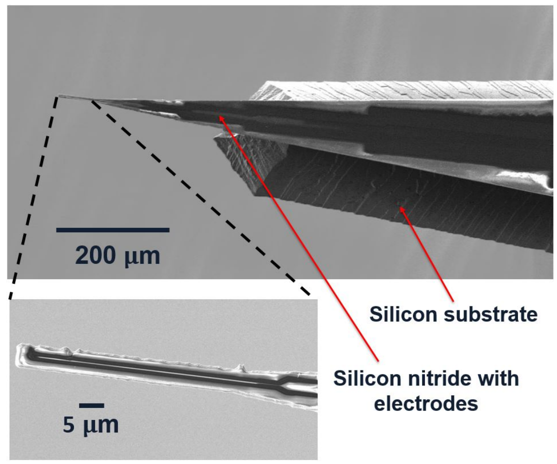

Figure 2: Scanning electron microscopy images of the fabricated thermocouple on a cantilever. The tip diameter is ∼5 μm. The suspended region is ∼451 μm long. The silicon substrate seen underneath the nitride has (111) planes exposed everywhere.

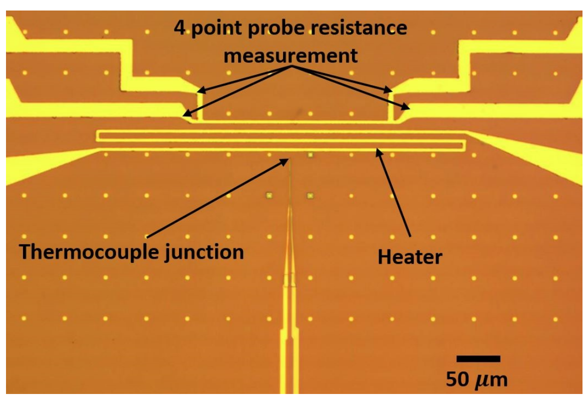

Figure 3: Calibration of the thermocouple junction is done using two thin film gold resistors that act as heater and temperature sensor. The measurements are done in a temperature controlled cryostat under high vacuum conditions ($< 10^{-6}$ bar).

process that follows the deposition of metal lines as shown in Fig. 1b, and prior to etching the bulk silicon. The calibration is done in a vacuum cryostat using a heater and a reference thermometer on-chip, as shown in Fig. 3. The heater line is 6 μm away from both the thermocouple junction and the reference junction. The close proximity of the sensors and vacuum conditions ensure heat conduction to be the dominant heat transfer mechanism. Therefore, an on-chip calibration method minimizes local convection currents, and provides an accurate calibration of both the reference thermometer and the thermocouple junction.

The calibration is a two-step process where a reference electrical resistance thermometer is itself first calibrated in a vacuum cryostat. The thermocouple is then calibrated in the second step using the calibrated resistance sensor. In the first step, the temperature coefficient of resistance (TCR) of the resistor line is calibrated by measuring changes in electrical resistance at different bath temperatures of the cryostat. The bath temperature of the cryostat has an accuracy of 1 mK. The electrical resistance of the resistor is measured using a 4-point probe method with two SR830 lock-in amplifiers. In the second step, a Keithley DC current source provided current to a serpentine heater line equidistant from the resistor and the thermocouple tip, as shown in Fig. 3. As a first approximation, the temperature rise at the thermocouple tip and the resistor respectively can be assumed to be the same. We later examine the validity of this assumption. A Keithley nanovoltmeter measured the potential difference across the thermocouple junction. The change in resistance at the resistor increases quadratically with the current at the heater, confirming that the resistance change is indeed due to increased temperatures. Figure 4 shows the resistance change with DC heating current.

The Seebeck coefficient of the thermocouple junction is obtained by fitting a straight line between the potential difference measured at the junction and the temperature rise measured at the resistor, as shown in Fig. 5. We obtained a Seebeck coefficient of 1.18 μV/K for the Au/Pd junction. This is comparable to previously reported estimates for few-nm thick metal lines [29]. Any differences in the observed Seebeck coefficient and previously reported values could be attributed to the thickness and quality of the metal films. The estimated error in the slope is 7.34 nV/K. This calibration process was performed on each probe. We found the Seebeck coefficient to vary within the range 0.8-1.3 μV/K over a wafer.

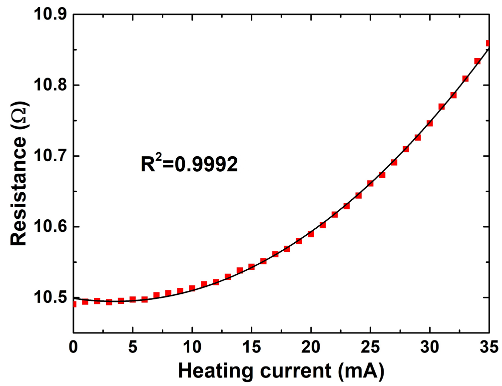

Figure 4: The resistance of the thin film resistor is plotted against the heating current. The data points shown in red squares fit well to a quadratic curve with a coefficient of determination (R^2) of 0.9992.

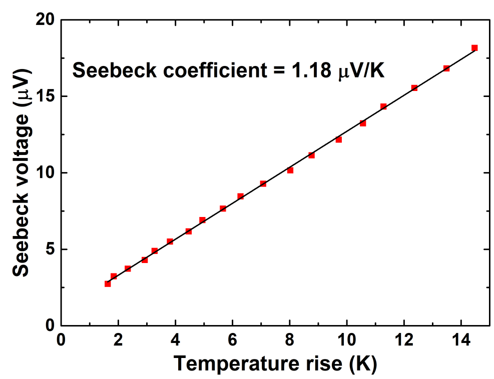

Figure 5: The Seebeck voltage across the Au/Pd junction is recorded as its temperature is increased by a heater. Temperature at the thermocouple junction is assumed to be the same as the thin film resistor. The data points are shown in red squares. Seebeck coefficient of the junction is the slope of a straight line fit to these points.

A subtle issue in the calibration arises from the fact that the temperatures at the thermocouple junction and thin film resistor may not be identical due to asymmetry. To investigate this issue, we performed finite element simulations of the calibration process in COMSOL to understand whether the asymmetry introduces a significant calibration error. The inset of Fig. 6 shows the geometry of the model. The serpentine heater line shown in Fig. 3 produces a temperature distribution that is symmetric along a (110) plane parallel to the length of the probe that bisects the heater and resistance sensor lines. For numerical simulations, we utilize this symmetry to model a 2D cross-section of the sample along the symmetry plane. While calibrating the sample in a vacuum cryostat, the sample was fixed to an adhesive tape on a chip holder. The exposed sides of the adhesive tape and the sample are the outer boundaries of this geometry. The cryostat's bath temperature ($T_{cryostat}$) yields the boundary condition at the bottom of the system. Adiabatic boundary conditions apply elsewhere since the system is in vacuum. The heater line is modeled as a constant heat source whose magnitude is equal to that of the heating power used in the measurements. The thermal properties of the materials are taken from the literature: $k_{Au\ film}$=225 W/mK [30], k_{SiN_x}=0.8 W/mK [31], k_{Si}=126.8 W/mK [31], and k_{tape}=1.4 W/mK [32]. The thermal contact resistance between the thin films (SiN_x/Si, Au/Cr/SiN_x) are on the order of 10^{-8} m^2K/W [33, 34], and are insignificant compared to the resistance of the adhesive tape ($\sim 10^{-3}$ m^2K/W) itself. The contact resistance on either side of the adhesive tape are also assumed to be negligible [35].

We first compare the temperature rise at the thin film resistor estimated from simulations against our measurements in Fig. 6 as a validation step. The simulated rise closely follows the measured values with a maximum deviation of 0.63 % at the highest heating current. This confirms that the thermal properties and boundary conditions used in the simulation adequately represent the calibration setup. Using this validated model, we now estimate the temperature differences between the thermocouple tip (T_{TC}) and thin film resistor ($T_{resistor}$) during calibration.

Figure 7 shows the difference in temperature between the resistor and the thermocouple junction at different heating currents. The bath temperature of the cryostat is fixed at $T_{cryostat}$ = 300 K in these calculations. For a 10 K rise in temperature at the junction, we find the error in calibration to be 54 mK. The error decreased to 27 mK for a 5 K rise from $T_{cryostat}$. The simulations

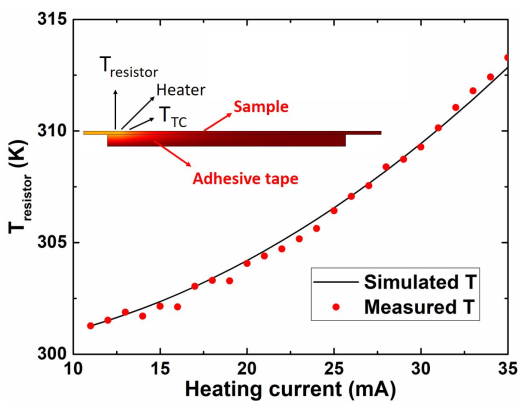

Figure 6: The simulated temperature rise at the resistor ($T_{resistor}$) is compared against measurements for increasing current at the heater. $T_{resistor}$ is obtained from 4pp resistance and the TCR of the thin film resistor. $T_{cryostat}$ = 300 K. (Inset) The geometry used for the simulation.

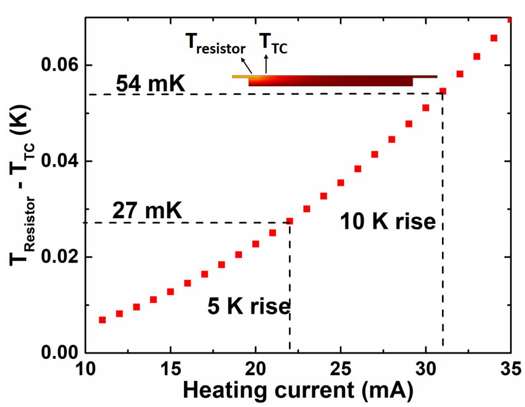

Figure 7: The temperature difference between the thermocouple tip and the thin film resistor is calculated at different heating currents. 31 mA heating current is estimated to produce 10 K rise at the resistance sensor. The error due to assuming symmetricity is 54 mK when the measured temperature rise from ambient ($T_{cryostat}$ = 300 K) is 10 K.

help to determine the maximum heating current to be used in calibration for a desired accuracy. For operating at 300±10 K, the accuracy of calibration is ±54 mK. We note that this figure is ∼2 orders of magnitude larger than the apparent temperature resolution of 0.85 mK possible with the probe when using a nanovoltmeter with 1 nV resolution. Further, we show experimentally in Section 4 that the noise floor is comparable to this calibration error. Hence, the calibration approach describe here helps to reduce the overall measurement uncertainty to approach the noise floor.

4. Thermal Response

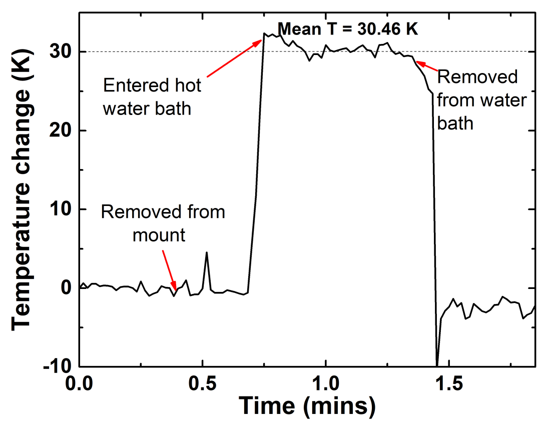

Figure 8: Transient temperature change measured in a hot water bath at a frequency of 1 Hz.

To observe the probe's temperature response after fabrication, we subjected it to a sudden temperature difference by dipping it in a water bath that was kept at 30 K above room temperature. The water bath's temperature was measured independently using a commercial Type-K thermocouple from Omega. Figure 8 shows transient temperatures at the probe, measured using a nanovoltmeter connected to the probe. From time $t < 0$ to $t = 0.4$ mins, the probe remained stationary, fixed to a mount. The probe was removed from the mount at $t = 0.4$ mins, and slowly moved towards the water bath. Sudden spikes in temperature readings were observed when the probe was manually moved. This is likely due to vibrations at the external solder joints while the probe was moved. As the probe touched the hot water surface at $t = 0.7$ mins, the measured temperature rose almost instantaneously on the time scale of Fig. 8. The probe measured an average temperature of 30.46 K during the 40 seconds it was inside the hot water bath. At t = 1.4 mins, the probe was removed from the water bath, which briefly induced evaporative cooling that resulted in a sudden decrease in temperature. We measured the noise floor in a quiescent water bath at room temperature to be around 42 mK over a few minutes. The noise floor increased in air to $\sim$211 mK. The temperature oscillations are possibly due to natural convection around the probe.

The data acquisition rate in the experiment shown in Fig. 8 is not sufficient to characterize the thermal response time of the probe. Typical thermal time constants of action potential pulses in neuron cells range from 4 - 100 ms [22]. To reliably measure stimuli at such time scales, we designed the thermal time constant of the sensor to be at least an order of magnitude lower. Here, we report numerical simulations in COMSOL to obtain the value. The geometry of the simulation is shown in the inset of Fig. 9. In this case, the symmetry plane defined in Section 3 is no longer a plane of symmetry since the width of the suspended probe gradually increases along the plane. Therefore, we extend the validated simulation model discussed in Section 3 to model a 3D geometry that resembles our probe. The 70 μm long probe tip was initially given a temperature of 313 K at t = 0 s. It is assumed to cool in water at 293 K for t > 0, and the time it takes to reach ambient conditions (293 K) is calculated. A natural convection boundary condition is applied to all the exposed surfaces except for the 70 μm tip region. We use a convection coefficient of 50 W/m^{2}K corresponding to natural convection in water. The convection coefficient along the microscale tip structure is typically much larger than at large scales. So, for the outer surfaces of the tip, we use a heat conduction boundary condition, pointed out by Hu et al [36] to be appropriate for microfabricated structures. The specific heat capacity of the materials used in the model are taken from the literature: $C_{\mathrm{Metal\ film}}$=0.3 J/kgK [37], $C_{\mathrm{SiN_x}}$=370 J/kgK [38], and C_{Si}=672 J/kgK [39]. Other required material properties are the same as discussed in Section 3.

We solved a transient three-dimensional heat conduction equation using the finite element method. A snapshot of the temperature profile at t = 5 μs is

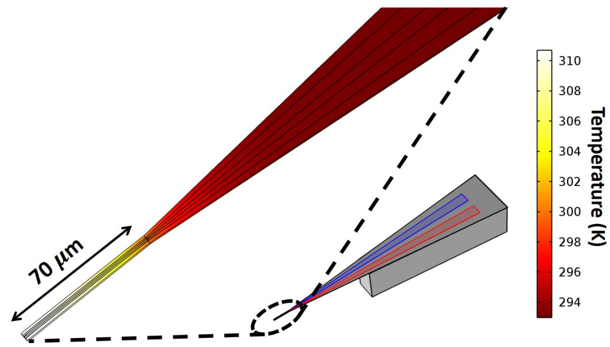

Figure 9: The simulated temperature contour of the probe at t = 5 μs. An initial temperature of 313 K is applied to the tip, while the ambient is at 293 K. (Inset) The geometry used for the simulation.

shown in Fig. 9. We calculate the temperature at the thermocouple tip over time as shown in Fig. 10. The thermal time constant of the probe is the time taken to change the temperature by a factor of $1/e$. From Fig. 10, the value is 32 μs, which is comparable to and better than the typical time constants of microscale thermal probes [23, 19]. The material and the small length scales of our thermocouple probe thus make it possible to have a thermal response time that is a few orders of magnitude smaller than the stimuli in a typical neuron cell [22].

5. Conclusion

In summary, we fabricated a thermocouple junction of 1 μm diameter in a silicon nitride cantilever of tip diameter 5 μm to serve as an intracellular thermometer. The low thermal conductivity, high stiffness and chemical inertness of silicon nitride make it a good choice for such a probe. We calibrated the thermocouple using an on-chip resistance sensor in a vacuum cryostat to obtain a calibration accuracy of $\pm$54 mK. A detailed error analysis of the calibration process shows that the accuracy can be further improved by limiting the heating current used for calibration. We demonstrated the use of the probe in an aqueous environment and found the noise floor to be 42 mK and comparable

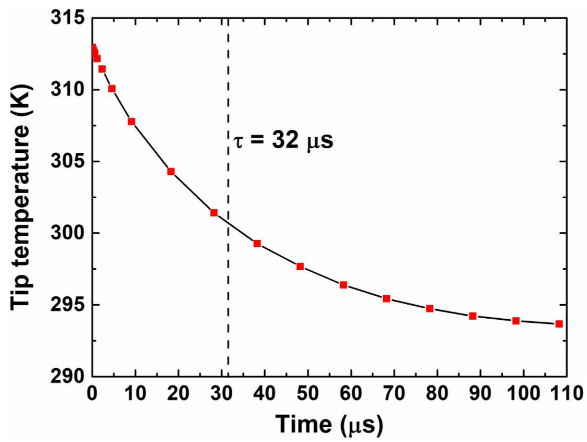

Figure 10: The simulated tip temperatures plotted against time as the probe cools down in water. The simulated points are shown in red squares. An exponential line fit to these points is used to obtain the thermal time constant of the probe.

to the calibration error. The sensor has a low thermal mass with a calculated thermal time constant of 32 μs, much smaller than the critical time constant of a neuron. Future experimental work will target *in vitro* thermometry in neurons with faster data acquisition rate. This work advances the design and fabrication of thermometers for intracellular measurements.

Acknowledgment

This work was supported in part by a grant from the C. J. Gauthier Program for Exploratory Studies of the Department of Mechanical Science and Engineering at the University of Illinois. This work was partly carried out in Micro Nano Technology Laboratory (MNTL), and Frederick Seitz Materials Research Laboratory (FS-MRL) at the University of Illinois, Urbana, IL.

References

[1] I. Watanabe, S. Okada, Effects of temperature on growth rate of cultured mammalian cells (L5178Y), The Journal of cell biology 32 (2) (1967) 309–323.

[2] Invited Review: Effects of heat and cold stress on mammalian gene expression, Journal of Applied Physiology 92 (4) (2002) 1725–1742, pMID: 11896043. doi:10.1152/japplphysiol.01143.2001.

[3] A thermodynamic approach to the problem of stabilization of globular protein structure: A calorimetric study, Journal of Molecular Biology 86 (3) (1974) 665 – 684. doi:https://doi.org/10.1016/0022-2836(74)90188-0.

[4] G. N. Somero, Proteins and temperature, Annual review of physiology 57 (1) (1995) 43–68.

[5] E. Tanaka, M. Yamamura, A. Yamakawa, T. Fujise, S. Nakano, Microcalorimetric measurements of heat production in isolated rat brown adipocytes., Biochemistry international 26 (5) (1992) 873–877.

[6] U. R. Acharya, E. Y.-K. Ng, J.-H. Tan, S. V. Sree, Thermography based breast cancer detection using texture features and support vector machine, Journal of medical systems 36 (3) (2012) 1503–1510.

[7] A. Helmy, M. Holdmann, M. Rizkalla, Application of thermography for non-invasive diagnosis of thyroid gland disease, IEEE transactions on biomedical engineering 55 (3) (2008) 1168–1175.

[8] C. Guy, F. Kaplan, J. Kopka, J. Selbig, D. K. Hincha, Metabolomics of temperature stress, Physiologia plantarum 132 (2) (2008) 220–235.

[9] B. B. Lowell, B. M. Spiegelman, Towards a molecular understanding of adaptive thermogenesis, Nature 404 (6778) (2000) 652–660.

[10] K. Okabe, N. Inada, C. Gota, Y. Harada, T. Funatsu, S. Uchiyama, Intracellular temperature mapping with a fluorescent polymeric thermometer and fluorescence lifetime imaging microscopy, Nature communications 3 (2012) 705.

[11] I. Tasaki, T. Nakaye, Heat generated by the dark-adapted squid retina in response to light pulses, Science 227 (1985) 654–656.

[12] P. Lctourncau, T. Shattuck, A. Ressler, Cellular and molecular mechanisms of drug dependence, Cell Motility 8 (1987) 193.

[13] Y. Zhao, J. A. Boulant, Temperature effects on neuronal membrane potentials and inward currents in rat hypothalamic tissue slices, The Journal of Physiology 564 (1) (2005) 245–257. `doi:10.1113/jphysiol.2004.075473`.

[14] J. S. Donner, S. A. Thompson, M. P. Kreuzer, G. Baffou, R. Quidant, Mapping Intracellular Temperature Using Green Fluorescent Protein, Nano Letters 12 (4) (2012) 2107–2111, pMID: 22394124. `arXiv:http://dx.doi.org/10.1021/nl300389y`, `doi:10.1021/nl300389y`.

[15] R. Tanimoto, T. Hiraiwa, Y. Nakai, Y. Shindo, K. Oka, N. Hiroi, A. Funahashi, Detection of temperature difference in neuronal cells, Scientific reports 6.

[16] G. Baffou, H. Rigneault, D. Marguet, L. Jullien, A critique of methods for temperature imaging in single cells, Nature methods 11 (9) (2014) 899.

[17] G. Fish, O. Bouevitch, S. Kokotov, K. Lieberman, D. Palanker, I. Turovets, A. Lewis, Ultrafast response micropipette-based submicrometer thermocouple, Review of scientific instruments 66 (5) (1995) 3300–3306.

[18] M. S. Watanabe, N. Kakuta, K. Mabuchi, Y. Yamada, Micro-thermocouple probe for measurement of cellular thermal responses, in: 2005 IEEE Engineering in Medicine and Biology 27th Annual Conference, 2005, pp. 4858–4861. `doi:10.1109/IEMBS.2005.1615560`.

[19] R. Shrestha, T.-Y. Choi, W. Chang, D. Kim, A high-precision micropipette sensor for cellular-level real-time thermal characterization, Sensors 11 (9) (2011) 8826–8835.

[20] C. Wang, R. Xu, W. Tian, X. Jiang, Z. Cui, M. Wang, H. Sun, K. Fang, N. Gu, Determining intracellular temperature at single-cell level by a novel thermocouple method, Cell research 21 (10) (2011) 1517.

[21] W. Tian, C. Wang, J. Wang, Q. Chen, J. Sun, C. Li, X. Wang, N. Gu, A high precision apparatus for intracellular thermal response at single-cell level, Nanotechnology 26 (35) (2015) 355501.

[22] L. Tauc, Site of origin and propagation of spike in the giant neuron of Aplysia, The Journal of General Physiology 45 (6) (1962) 1077–1097. `doi:10.1085/jgp.45.6.1077`.

[23] S. Herth, M. Giesguth, W. Wedel, G. Reiss, K.-J. Dietz, Thermomicrocapillaries as temperature biosensors in single cells, Applied Physics Letters 102 (10) (2013) 103505.

[24] G. S. Wilson, R. Gifford, Biosensors for real-time in vivo measurements, Biosensors and Bioelectronics 20 (12) (2005) 2388 – 2403, 20th Anniversary of Biosensors and Bioelectronics. `doi:10.1016/j.bios.2004.12.003`.

[25] F. Yu, J. Liu, X. Zhang, A.-L. Lin, N. Khan, Y. Pan, N. Gao, Q. Zou, J. Jeon, Design, fabrication, and characterization of polymer-based cantilever probes for atomic force microscopes, Journal of Vacuum Science & Technology B, Nanotechnology and Microelectronics: Materials, Processing, Measurement, and Phenomena 34 (6) (2016) 06KI01. `doi:10.1116/1.4960726`.

[26] R. K. Ulrich, W. Brown, S. Ang, S. Yi, J. Sweet, D. Peterson, PECVD silicon and nitride postbond films for protecting bondpads, bonds and bondwires from corrosion failure, in: Electronic Components and Technology Conference, 1991. Proceedings., 41st, IEEE, 1991, pp. 738–744.

[27] E. Cianci, A. Coppa, V. Foglietti, Youngs modulus and residual stress of DF PECVD silicon nitride for MEMS free-standing membranes, Microelectronic engineering 84 (5) (2007) 1296–1299.

[28] A. A. Sharp, A. M. Ortega, D. Restrepo, D. Curran-Everett, K. Gall, In vivo penetration mechanics and mechanical properties of mouse brain tissue at micrometer scales, IEEE Transactions on Biomedical Engineering 56 (1) (2009) 45–53.

[29] G. P. Szakmany, P. M. Krenz, L. C. Schneider, A. O. Orlov, G. H. Bernstein, W. Porod, Nanowire Thermocouple Characterization Platform, IEEE Transactions on Nanotechnology 12 (3) (2013) 309–313. `doi:10.1109/TNANO.2013.2247057`.

[30] G. Langer, J. Hartmann, M. Reichling, Thermal conductivity of thin metallic films measured by photothermal profile analysis, Review of Scientific Instruments 68 (3) (1997) 1510–1513.

[31] S.-M. Lee, D. G. Cahill, Heat transport in thin dielectric films, Journal of applied physics 81 (6) (1997) 2590–2595.

[32] Thor labs thermally conductive double-sided tape specifications Sheet TCDT1.
URL `https://www.thorlabs.com/thorproduct.cfm?partnumber=TCDT1`

[33] S. Huang, X.-d. Ruan, X. Fu, H.-y. Yang, Measurement of the thermal transport properties of dielectric thin films using the micro-Raman method, Journal of Zhejiang University-SCIENCE A 10 (1) (2009) 7–16.

[34] T. Jeong, J.-G. Zhu, S. Chung, M. R. Gibbons, Thermal boundary resistance for gold and CoFe alloy on silicon nitride films, Journal of Applied Physics 111 (8) (2012) 083510.

[35] M. Chertok, M. Fu, M. Irving, C. Neher, M. Shi, K. Tolfa, M. Tripathi, Y. Vinson, R. Wang, G. Zheng, Thermal and tensile strength testing of thermally-conductive adhesives and carbon foam, Journal of Instrumentation 12 (01) (2017) P01010.

[36] X. J. Hu, A. Jain, K. E. Goodson, Investigation of the natural convection boundary condition in microfabricated structures, International Journal of Thermal Sciences 47 (7) (2008) 820–824.

[37] D. Denlinger, E. Abarra, K. Allen, P. Rooney, M. Messer, S. Watson, F. Hellman, Thin film microcalorimeter for heat capacity measurements from 1.5 to 800 K, Review of Scientific Instruments 65 (4) (1994) 946–959.

[38] B. Zink, F. Hellman, Specific heat and thermal conductivity of low-stress amorphous Si–N membranes, Solid State Communications 129 (3) (2004) 199–204.

[39] A. Okhotin, A. Pushkarskii, V. Gorbachev, Thermophysical properties of semiconductors, Atom Publ, House, Moscow.